The 8th Scandinavian Conference on Image Analysis, Tromso, Norway, May 25-28, 1993.

Determining Shape of Specular Surfaces

Zengfu Wang* and Seiji Inokuchi**

*Laboratories of Image Information Science and Technology, Toyonaka, Osaka, 565, Japan
**Faculty of Engineering Science, Osaka University, Toyonaka, Osaka, 560, Japan

Abstract

A new method for determining the shape of specular surfaces is presented in this paper. Our approach reconstructs the shape of specular surfaces from a relationship between the surrounding environment and the observed images of specular surfaces. A prototype system has been implemented. The experimental results show that the proposed method is effective to the reconstruction of specular objects of curved surfaces.

1 Introduction

For many practical tasks in robot vision, a key step is to extract the three dimensional shape of the object surface. This involves the analysis of images resulting from the reflection of light. Most previous approaches to this problem have assumed that surfaces are Lambertian, that is, incident light is scattered by the surface so that the perceived brightness is independent of the direction of view. It is difficult to determine the shape of specular surfaces that have a dominant specular component of reflection.

In resent years, the importance of understanding and using specular reflections has been realized, and considerable effort is being directed in this area [1] [2]. In the meantime, the shape extraction techniques for specular surfaces have been developed. K.Koshikawa [3] has described a model based way of detecting surface normals from the polarization angles of reflected light. K.Ikeuchi [4] has proposed to recover the surface orientations from the specular components of reflectance under different illuminations. His approach utilizes an extended light source which is brightness encoded, and assumes that the object is small compared with the distance to the source and the image-forming system. The approach requires measurement of reflected brightness with sufficient accuracy to isolate a particular position in the source field. A.C.Sanderson and S.K.Nayar et al. [5] [6] have proposed a "structured highlight" approach which utilizes an array of point sources to illuminate the specular surfaces and can obtain the corresponding three dimensional shape information from the resulting highlight patterns on a fixed camera image. Their approach needs a special illuminating unit to guarantee that each surface element of an object within the field may be scanned. S.K.Nayar et al. [7] have presented a photometric sampling method for determining the shape of hybrid surfaces. Their method can recover surface shape and reflectance properties simultaneously from a sequence of observed images of the object surface which is illuminated by extended light sources and is viewed from a single direction, but the measuring process must be done in a darkroom condition.

In this paper we describe a new method for determining the shape of specular surfaces. Here, the word "specular surface" means a kind of mirror-like surface which has a dominant specular component of reflection. Suppose that the position information of the surrounding environment is known, we can prove that the shape of specular surfaces can be reconstructed from a relationship between the surrounding environment and the corresponding observed images of specular surfaces. In this work, four constraints are introduced: view-line constraint, Snell's law, smoothness constraint and ideal imaging constraint. The view-line constraint and Snell's law are two basic constraints. They give the necessary conditions of the solution, but are not sufficient to determine the surfaces uniquely. To further restrict the solution, some additional constraints are imposed. First, we consider a simple case when a seed point on the specular surface may be used. We will introduce two more constraints to obtain the surface shape. One method uses the smoothness constraint, the other one is based on the ideal imaging constraint. Each of the above two methods gives an acceptable but may not a good solution to the problem. To improve the reconstruction result, the shape from smoothness constraint and the shape from ideal imaging constraint will then be fused to get a solution with maximum certainty factor. Then we consider a general case when no seed point on the specular surface can be used. We will show how to get a better solution by fusing data from two images. A prototype system has been implemented to verify the proposed methods. We will present the experimental results on synthetic and real data and provide some concluding remarks.

2 Basic definitions and equations

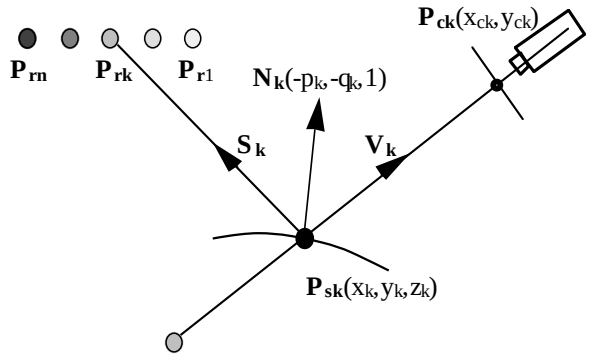

Fig.1

To extract the shape of the specular surface of interest, we utilize the position information of the surrounding environment and the observed images of the specular surface. As shown in Fig.1, the surrounding environment is considered as a set of reference points $\mathbf{P}_{rk}(k=1,2,...n)$, where the position information of each reference point is assumed to be known. A fixed camera is used to observe the specular surface. Corresponding to each reference point $\mathbf{P}_{rk}$, the emitted light rays will be reflected off the specular surface. If the reference point $\mathbf{P}_{rk}$ is positioned such that a part of the reflected light rays from the specular surface is admitted by the camera, an image $\mathbf{P}_{ck}$ will be formed on the camera image plane. In this paper, the point of interest on the specular surface corresponding to $\mathbf{P}_{ck}$ is called the observing point $\mathbf{P}_{sk}$ which is defined as the intersection of the specular surface and the view-line through $\mathbf{P}_{ck}$.

2.1 Camera parameter

There is a relationship between a point $\mathbf{P}(x,y,z)$ and the corresponding image $\mathbf{P}_c(xc,yc)$ on the camera image plane [8].

$$\begin{bmatrix} H_c x_c \\ H_c y_c \\ H_c \end{bmatrix} = \begin{bmatrix} C_{11}C_{12}C_{13}C_{14} \\ C_{21}C_{22}C_{23}C_{24} \\ C_{31}C_{32}C_{33}C_{34} \end{bmatrix} \begin{bmatrix} x \\ y \\ z \\ 1 \end{bmatrix} \quad (1)$$

Where matrix $[C_{ij}]_{3\times 4}$ is called camera parameter, it can be determined by using a calibration procedure.

2.2 View-line constraint

The view-line constraint restricts the position of the observing point, that is, the observing point must lie on the corresponding view-line. from (1), we have

$$l_{k1}x_k+m_{k1}y_k+n_{k1}z_k+t_{k1} = 0 \quad (2)$$
$$l_{k2}x_k+m_{k2}y_k+n_{k2}z_k+t_{k2} = 0 \quad (3)$$

Where

$l_{k1} = C_{11} - C_{31}x_{ck}$, $m_{k1} = C_{12} - C_{32}x_{ck}$
$n_{k1} = C_{13} - C_{33}x_{ck}$, $t_{k1} = C_{14} - C_{34}x_{ck}$
$l_{k2} = C_{21} - C_{31}y_{ck}$, $m_{k2} = C_{22} - C_{32}y_{ck}$
$n_{k2} = C_{23} - C_{33}y_{ck}$, $t_{k2} = C_{24} - C_{34}y_{ck}$

Equations (2) and (3) are called view-line equations.

2.3 Snell's law

Snell's law restricts the surface normal at observing point.

From (2) and (3), the direction of the view-line through $\mathbf{P}_{sk}(x_k,y_k,z_k)$ can be expressed as follows.

$$(l_k,m_k,n_k) = \begin{vmatrix} \mathbf{-i} & \mathbf{-j} & \mathbf{-k} \\ l_{k1} & m_{k1} & n_{k1} \\ l_{k2} & m_{k2} & n_{k2} \end{vmatrix} \quad (4)$$

Where + direction is referred to as such a direction, which points toward camera from $\mathbf{P}_{sk}$.

Under above definitions, Snell's law is written as

$$\mathbf{S}_k \cdot \mathbf{N}_k = \mathbf{N}_k \cdot \mathbf{V}_k \quad (5)$$
$$(\mathbf{S}_k \times \mathbf{V}_k) \cdot \mathbf{N}_k = 0 \quad (6)$$

Where $\mathbf{S}_k$ is the unit vector of the incident direction at $\mathbf{P}_{sk}$, $\mathbf{V}_k$ is the unit vector of the reflected direction at $\mathbf{P}_{sk}$, while $\mathbf{N}_k$ is the surface normal at $\mathbf{P}_{sk}$. They are defined as follows:

$$\mathbf{S}_k = (\mathbf{P}_{rk} - \mathbf{P}_{sk}) / \|\mathbf{P}_{rk} - \mathbf{P}_{sk}\| \quad (7)$$
$$\mathbf{V}_k = (l_k,m_k,n_k) / \sqrt{l_k^2+m_k^2+n_k^2} \quad (8)$$
$$\mathbf{N}_k = (-p_k,-q_k,1) / \sqrt{p_k^2+q_k^2+1} \quad (9)$$

Where

$$p_k = \left(\frac{\partial z}{\partial x}\right)_{z=z_k}, \quad q_k = \left(\frac{\partial z}{\partial y}\right)_{z=z_k}$$

From (5), (6), (7), (8) and (9) we can prove that $\mathbf{N}_k$ is a function of $\mathbf{P}_{sk}$.

$$p_k = p_k(\mathbf{P}_{sk}) , \quad q_k = q_k(\mathbf{P}_{sk}) \quad (10)$$

So if the position information of the observing point $\mathbf{P}_{sk}$ is given, the surface normal at $\mathbf{P}_{sk}$ can be computed from (10).

The above view-line constraint and Snell's law restrict the solution as follows: that is, when the position of a point on the specular surface is known, the corresponding surface normal can be derived from (10). Inversely when the surface normal is given, the corresponding position

can be derived also. However, the two constraints are not sufficient to determine the surface uniquely. To obtain the shape of the specular surface, we need impose some additional constraints.

3 Shape reconstruction using an known point on the surface

When a seed point on the specular surface can be used, we can estimate the adjacent area on the specular surface from the known point. Then a propagation processing will help us to recover the entire shape of the specular surface.

3.1 Shape reconstruction based on smoothness constraint

The smoothness constraint shows that if the specular surface is smooth, the normal surface must vary continuously. So the surface normal at a point can be estimated from the one of an adjacent point.

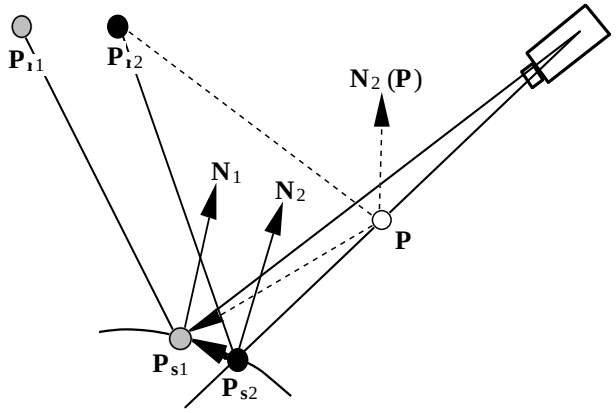

Fig.2 Smoothness constraint

The smoothness constraint is represented by

$$\lim_{\mathbf{P}_{s2}\to\mathbf{P}_{s1}} \mathbf{l}(\mathbf{P}_{s2}, \mathbf{P}_{s1})\cdot\mathbf{N}_1 = 0 \qquad (11)$$

$$\lim_{\mathbf{P}_{s2}\to\mathbf{P}_{s1}} \mathbf{l}(\mathbf{P}_{s2}, \mathbf{P}_{s1})\cdot\mathbf{N}_2 = 0 \qquad (12)$$

Where $\mathbf{P}_{s1}$ and $\mathbf{P}_{s2}$ are two points on the specular surface respectively. $\mathbf{l}(\mathbf{P}_{s1},\mathbf{P}_{s2})$ represents the unit vector from $\mathbf{P}_{s2}$ to $\mathbf{P}_{s1}$. $\mathbf{N}_1$ and $\mathbf{N}_2$ are the surface normals at $\mathbf{P}_{s1}$ and $\mathbf{P}_{s2}$ respectively. As shown in Fig.2, when $\mathbf{P}_{s2}$ approaches $\mathbf{P}_{s1}$ along any route on the surface, the surface normal at $\mathbf{P}_{s2}$ changes along the route but will approach the one at $\mathbf{P}_{s1}$ limitlessly at last. That is, when $\mathbf{P}_{s2}$ approaches $\mathbf{P}_{s1}$ sufficiently, $\mathbf{l}(\mathbf{P}_{s1},\mathbf{P}_{s2})$ will be orthogonal approximately to the surface normals at $\mathbf{P}_{s1}$ and $\mathbf{P}_{s2}$ simultaneously.

Let $\mathbf{P}_{s1}$ and $\mathbf{P}_{s2}$ be two adjacent points on the specular surface and $\mathbf{P}_{s1}$ be known. We next show how to recover $\mathbf{P}_{s2}$ from $\mathbf{P}_{s1}$ using the smoothness constraint.

From (10) we can calculate the surface normal at $\mathbf{P}_{s1}$ using $\mathbf{P}_{r1}$, $\mathbf{P}_{s1}$ and $\mathbf{P}_{c1}$, where p1 and q1 are constants. Similarly we can represent the surface normal at $\mathbf{P}_{s2}$ using $\mathbf{P}_{r2}$, $\mathbf{P}_{s2}$ and $\mathbf{P}_{c2}$, where the resulting p2 and q2 will be a function of $\mathbf{P}_{s2}$. When $\mathbf{P}_{s2}$ is given, p2 and q2 can be calculated from $\mathbf{P}_{r2}$ and $\mathbf{P}_{c2}$.

Consequently the surface normal at $\mathbf{P}_{s1}$, $\mathbf{N}_1$, is a constant vector and the surface normal at $\mathbf{P}_{s2}$, $\mathbf{N}_2$, is a variable vector which can be expressed as a function of $\mathbf{P}_{s2}$.

Similarly, the unit vector from $\mathbf{P}_{s2}$ to $\mathbf{P}_{s1}$ can be expressed as a function of $\mathbf{P}_{s2}$.

To recover $\mathbf{P}_{s2}$, we use the smoothness constraint. Since the $\mathbf{P}_{s2}$ is constrained to lie on the corresponding view-line, we introduce the following cost function

$$E_{smooth}(\mathbf{P}) = \max\left(\left|\mathbf{l}(\mathbf{P}_{s1}-\mathbf{P})\cdot\mathbf{N}_1\right| , \left|\mathbf{l}(\mathbf{P}_{s1}-\mathbf{P})\cdot\mathbf{N}_2(\mathbf{P})\right| \right) \qquad \mathbf{P}\in D$$

Where D shows the search range which is defined as an interval on the view-line containing $\mathbf{P}_{s2}$. $\mathbf{P}$ is a dynamic point on it. When the local shape of the surface is a plane, the above cost function E_{smooth} will have a zero value ideally at $\mathbf{P}_{s2}$. In other cases, E_{smooth} will take a minimum at $\mathbf{P}_{s2}$.

It can be proved that the above cost function E_{smooth} is a single value function of $\mathbf{P}$. So $\mathbf{P}_{s2}$ can be estimated by finding the $\mathbf{P}$ which gives a minimum of E_{smooth}.

In this paper, the above method is called **SC**'method (reconstruction method based on **S**moothness **C**onstraint).

3.2 Shape reconstruction based on ideal imaging constraint

Before state the ideal imaging constraint, let us give some definitions at first. Suppose that there are an optical surface and a reference point source in space. The emitted light rays from the reference point source will be reflected off the surface. If the reflected light rays intersect each other at a point of space, we say the surface forms an ideal image corresponding to the reference point. The surface is called ideal imaging surface, and the point is called image point corresponding to the surface and the reference point. The examples of optical surface with the above property include plane mirror, hyperboloid mirror and ellipsoid mirror. In the plane case, the image point and the corresponding reference point will position symmetrically with respect to the plane. In hyperboloid and ellipsoid cases, the image point and the corresponding reference point will lie on the two focus positions respectively. Generally speaking, for a specular surface with an arbitrary shape, the above ideal imaging property is not

satisfied. But in the mirror case, the reflected rays seen by the camera come from the local area on the surface only, so when the local shape can be approximated by an ideal imaging surface, the corresponding image will be seen.

The ideal imaging constraint shows that if the local shape of the specular surface can be approximated by an ideal imaging surface, the mirror images of the corresponding reference points viewed from the local shape can be computed. Once the mirror images are estimated, the possible surface may be determined by a relationship between the reference points and the corresponding mirror images.

As shown in Fig.3, we will specify the ideal imaging constraint by an example of the plane case.

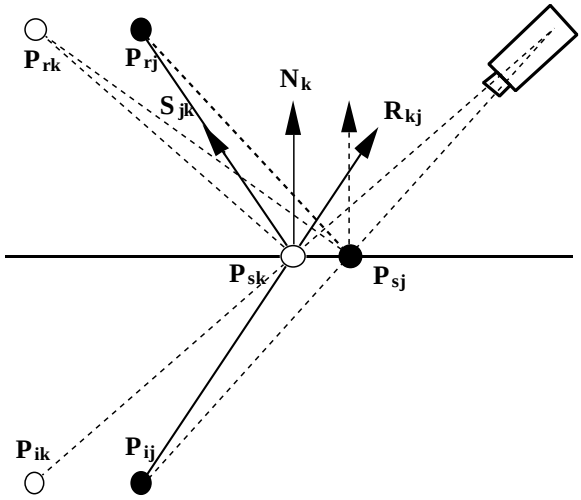

Fig.3 Ideal imaging constraint

The ideal imaging constraint is written as

$$\begin{cases} \mathbf{S}_{jk} \cdot \mathbf{N}_k = \mathbf{N}_k \cdot \mathbf{R}_{kj} \\ (\mathbf{S}_{jk} \times \mathbf{R}_{kj}) \cdot \mathbf{N}_k = 0 \end{cases} \quad j,k = 1,2 \ldots n \qquad (13)$$

Where $\mathbf{S}_{jk}$ shows an incident vector from $\mathbf{P}_{sk}$ to $\mathbf{P}_{rj}$, $\mathbf{N}_k$ shows the surface normal at $\mathbf{P}_{sk}$, $\mathbf{R}_{kj}$ shows a reflected vector from $\mathbf{P}_{ij}$ to $\mathbf{P}_{sk}$, while n shows the number of the image points seen from the local shape. (13) shows that among $\mathbf{S}_{jk}$, $\mathbf{N}_k$ and $\mathbf{R}_{kj}$, Snell's law holds. Where $\mathbf{R}_{kj}$ (j =1,2,...n) correspond to imaginary reflected vectors. All of the reflected vectors except $\mathbf{R}_{kk}$ can not be seen by the camera. But according to the definition of the ideal imaging, these reflected vectors should be agreed with the real reflected ones. In the next, we will use this point to estimate the real reflected vectors.

Now let us consider how to recover $\mathbf{P}_{s2}$ from $\mathbf{P}_{s1}$.

First, we need estimate the position of the image points corresponding to the reference points. This can be done by the following method. As shown in Fig.4, we consider the estimation of $\mathbf{P}_{i2}$. The incident rays from the reference point $\mathbf{P}_{r2}$ are reflected off the surface. By definition, the reflected ray at the known point $\mathbf{P}_{s1}$ will pass through the image point $\mathbf{P}_{i2}$. On the other hand, the reflected ray seen by the camera will pass through the same point $\mathbf{P}_{i2}$ too. So the image point $\mathbf{P}_{i2}$ can be computed by finding the intersection of the two rays. Similarly, the other image points can be found by the same method. In three dimensional case we have a trouble, since the exact intersection between the two rays is unlikely to occur. In such a case, the point on the view-line, at which the distance between the above two rays has a minimum, is selected to be the corresponding image point.

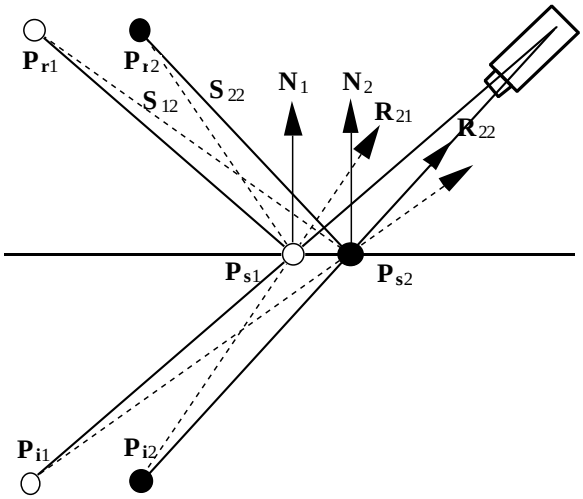

Fig.4 Shape reconstruction based on ideal imaging constraint

Similar to **SC**'method case, we introduce the following cost function

$$E_{ideal}(\mathbf{P}) = \sum_{k=1}^{n} ((\mathbf{S}_{k2} \cdot \mathbf{N}_2 - \mathbf{N}_2 \cdot \mathbf{R}_{2k})^2 + ((\mathbf{S}_{k2} \times \mathbf{R}_{2k}) \cdot \mathbf{N}_2)^2) \qquad \mathbf{P} \in D$$

When the local shape at point $\mathbf{P}_{s2}$ has a plane shape, the cost function has a zero value ideally at $\mathbf{P}_{s2}$. In other cases, the cost function will take a minimum at $\mathbf{P}_{s2}$. So $\mathbf{P}_{s2}$ can be estimated by finding the $\mathbf{P}$ which gives a minimum of E_{ideal}.

The above method is called **IC**'method (reconstruction method based on ideal **I**maging **C**onstraint).

3.3 Refining reconstruction result by hypothesis unification

The two proposed methods mentioned can give an estimation of the specular surface, but don't always give

good results. The reason is as follows. In **SC**'method case, no knowledge about local curvature of the specular surface may be used. The recovered shape is enforced to be as smooth as possible. As a result, when the curvature varies abruptly, accumulation of quantization errors brings a difference between the recovered shape and the real shape. In **IC**'method case, as only local shape is considered, the smoothness constraint may not be satisfied. Globally a wrong result may be obtained. So the performance of both **SC**'method and **IC**'method is limited.

To refine reconstruction result, we next show how to compensate for lack of knowledge in the above two cases. Where, a known point $\mathbf{P}_{s1}$ on the specular surface will be used as before. For simplicity, we only consider the reconstruction of an adjacent point $\mathbf{P}_{s2}$ on the specular surface. Our method, is called **HU**'method (reconstruction method based on **H**ypothesis **U**nification), contains two steps.

1. Create hypotheses corresponding to both **SC**'method and **IC**'method, where the corresponding certainty factors are defined as follows:

$$CF_{smooth}(\mathbf{P}) = 1 - E_{smooth}(\mathbf{P})$$

$$CF_{ideal}(\mathbf{P}) = 1 - \frac{E_{ideal}(\mathbf{P}) - \underset{\mathbf{P}\in D}{\mathrm{Min}}(E_{ideal}(\mathbf{P}))}{\underset{\mathbf{P}\in D}{\mathrm{Max}}(E_{ideal}(\mathbf{P})) - \underset{\mathbf{P}\in D}{\mathrm{Min}}(E_{ideal}(\mathbf{P}))}$$

2. Unify the created hypotheses by some method. There are two possible unification methods can be used. One is to select the hypothesis which has a bigger certainty factor. The other is to create a new hypothesis from the above two ones and use the new one to recover the specular surface. In this paper, we use the latter method. The new certainty factor is defined as

$$CF_{unify}(\mathbf{P}) = CF_{smooth}(\mathbf{P})\, CF_{ideal}(\mathbf{P})$$

It is a product of the two corresponding certainty factors. We found that the maximum value of CF_{unify} will correspond to such a point, at which both CF_{smooth} and CF_{ideal} take a bigger value but not a maximum value. In this way, the local shape of the specular surface and the smoothness constraint are fully used simultaneously, the oversmoothing as in **SC**'method case will be avoided. So compared with both **SC**'method and **IC**'method, the recovered shape will be more close to the real shape.

To recover the entire specular surface, the above unification processing will be propagated from known points to the adjacent area. Once an unified hypothesis is selected, the corresponding recovered point will be regarded as a new known point from which a propagation processing will be done in the neighborhood.

4 Shape from fusion of multi-image

The methods proposed in section 3 need a seed point on the specular surface whose position is referred to be known. When no point on the specular surface may be used, the above two methods can not be utilized directly. To obtain a correct solution, we should utilize some additional data. For example, we can use the measured data from the other objects on the scene to find an estimation of some seed point on the specular surface. We can also get a good estimation of the seed point by using a known reference plane.

In this paper, we propose another method. The method uses more than one image. The data from different view directions are fused to get a better result. Here we only consider the two images' case.

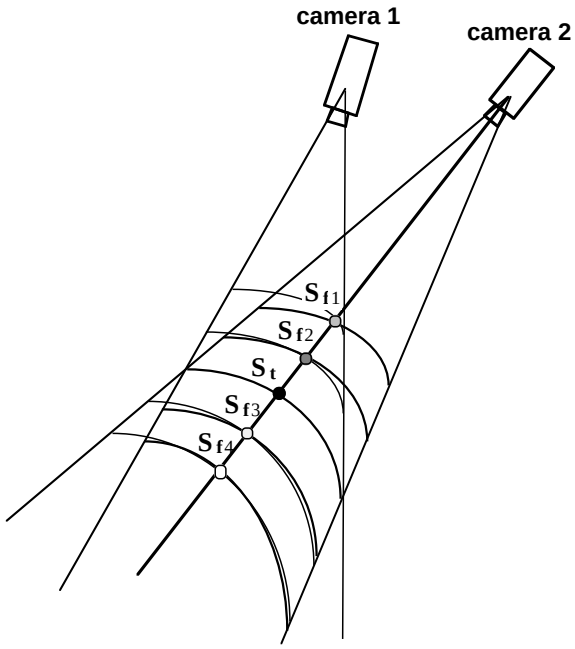

Fig.5 Concept of shape from fusion of two images

We noticed the following fact, that is, the position and the shape of a specular surface don't depend on the view direction. If the selected seed point is on the specular surface, the shapes obtained from the different view directions will be the same. On the other hand, if the selected seed point does not belong to the specular surface, the shapes obtained from the different view directions will be different. In this paper, the above fact is called invariability principle about position and shape.

We use the principle to get the correct shape of a specular surface. The concept is shown in Fig.5. Where $\mathbf{S}_t$, $\mathbf{S}_{fn}$ (n = 1,2,...) show the possible selected seed points which lie on the same view-line and $\mathbf{S}_t$ belongs to the specular surface. When we select $\mathbf{S}_t$ as a seed point, the reconstructed shapes from the two images will be the same. In other cases, the reconstructed shapes from the two images don't correspond.

So we can get an estimation of the correct shape of a specular surface as follows:

1. To each possible selected seed point, compute the corresponding shapes of the specular surface from the two images using **HU**'method.
2. Compare the difference between the reconstructed shapes from the two images.
3. Select the shape which has a best correspondence between the shapes from the two images as an estimation of the specular surface.

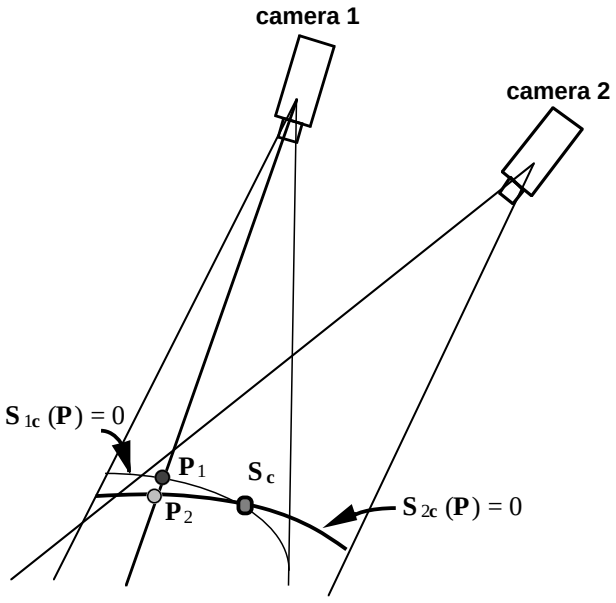

Fig.6 Definition of the correspondence between two surfaces

To evaluate the correspondence between the shapes from the two images, we introduce the following cost function:

$$E(S_{1c}) = \sum_{\mathbf{P}_1 \in \{\mathbf{P}:S_{1c}(\mathbf{P})=0\}} d(\mathbf{P}_1,\mathbf{P}_2) \qquad S_{1c} \in G \qquad (14)$$

Where, as shown in Fig.6, $\mathbf{S}_c$ shows a possible selected seed point. $S_{1c}(\mathbf{P})$ and $S_{2c}(\mathbf{P})$ are the corresponding reconstructed surfaces from image 1 and image 2 respectively. $\mathbf{P}_1$ is a point on $S_{1c}(\mathbf{P})$ and $\mathbf{P}_2$ shows the intersection of the corresponding view-line and the reconstructed surface $S_{2c}(\mathbf{P})$. $d(\mathbf{P}_1, \mathbf{P}_2)$ shows the distance between $\mathbf{P}_1$ and $\mathbf{P}_2$. When the corresponding $\mathbf{P}_2$ does not exist, $d(\mathbf{P}_1, \mathbf{P}_2)$ will take a bigger value. G shows a set of the reconstructed shapes from image 1. It is obvious that among the reconstructed shapes, the candidate corresponding to the minimum of the cost function will gives a good estimation of the real shape.

The above method considers the entire specular surface. When we pay our attention to a single point on the specular surface, we get an interesting special case. In this case, the invariability principle becomes the epipolar constraint. The corresponding cost function is defined as:

$$E(\mathbf{P}) = d(\mathbf{N}_1,\mathbf{N}_2) \qquad \mathbf{P} \in G \qquad (15)$$

Where G shows a view-line corresponding to the pixel of attention in image 1. $\mathbf{P}$ is a dynamic point on it. $\mathbf{N}_1$ and $\mathbf{N}_2$ are the surface normals at $\mathbf{P}$ estimated from the observed data of image 1 and image 2 respectively. $d(\mathbf{N}_1, \mathbf{N}_2)$ shows the difference between $\mathbf{N}_1$ and $\mathbf{N}_2$. It is obvious that when $\mathbf{P}$ is a point on the specular surface, the computed $\mathbf{N}_1$ and $\mathbf{N}_2$ will correspond. In other cases, the computed $\mathbf{N}_1$ and $\mathbf{N}_2$ don't correspond. So the real position of a point on the specular surface will be given by the point on the view-line which gives a minimum of (15). The corresponding surface normal will be given by $\mathbf{N}_1$ or $\mathbf{N}_2$. We found that the above proposed method determines the position and orientation locally. It is robust against noise. A parallel processing can be utilized to get the solution rapidly.

5 Experiments

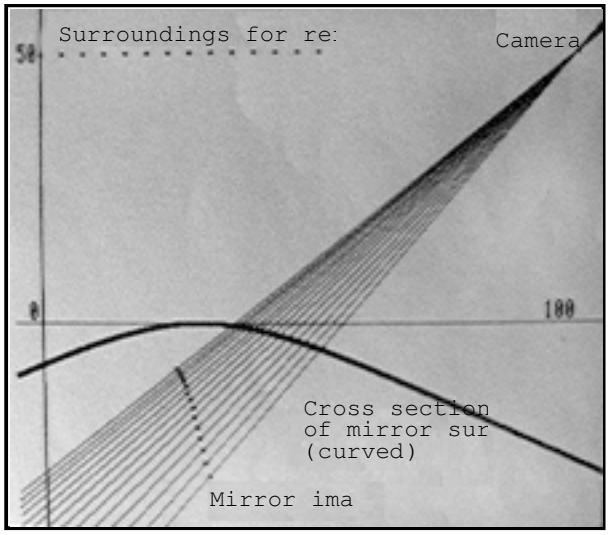

Fig.7 The configuration of the simulation system

To verify the proposed methods, the simulations have been performed. In this paper, we only represent the simulation results for cross section case. Fig.7 shows the configuration of the simulation system. Where the camera is positioned on the top-right side. The points in a straight line on the top-left side are referred to as reference points for surrounding environment.

The results of **SC**'method, **IC**'method and **HU**'method are shown in Fig.8, Fig.9 and Fig.10 respectively. We found that the **SC**'method gives a smooth surface which is close to but does not agree with the real shape, the **IC**'method can recover the local shape of specular surfaces very good, but can not give a good result about global shape and the **HU**'method gives an expected result.

Fig.8 Result of **SC**'method

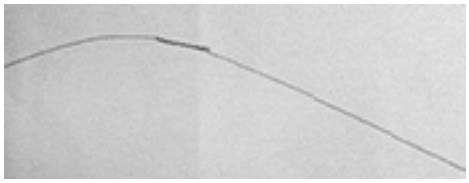

Fig.9 Result of **IC**'method

Fig.10 Result of **HU**'method

To illustrate that the proposed methods actually work, a prototype system has been implemented. The system is composed of some projectors and plane shaped screens. Grid patterns generated by projectors are projected on plane shaped screens to simulate known surroundings. To obtain a wide range of view, some plane shaped screens are arranged to form a shape of cube. The measured specular object is set inside the cube shaped screen. The screens have a front scattered property. When the patterns are projected by an LCD projector to the back of a plane shaped screen, at the front of the screen the patterns corresponding to the projected ones will be seen.

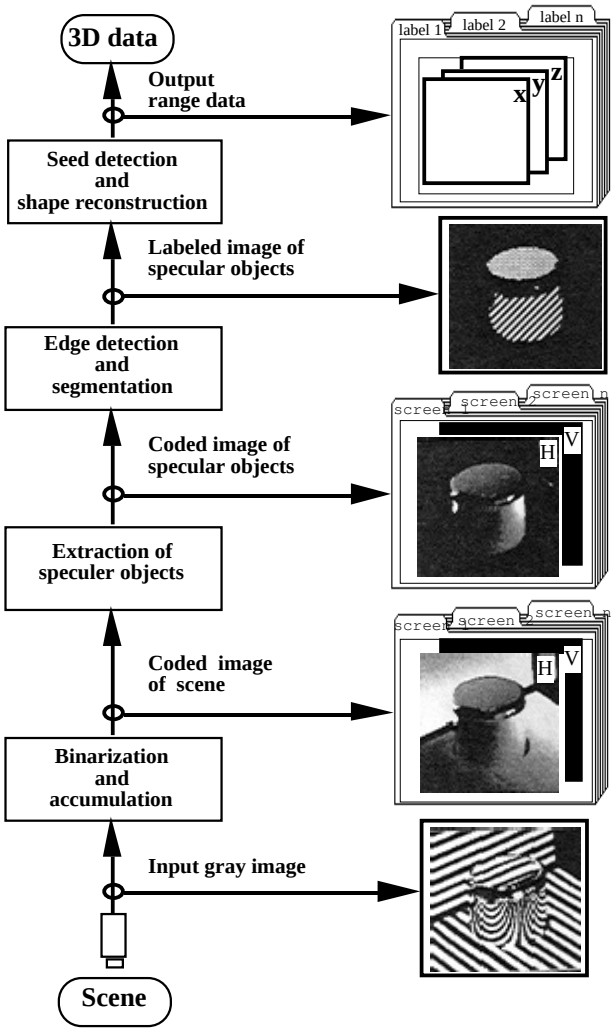

Fig.11 Processing flow of the system

The processing flow of the system is shown in Fig.11. It contains four steps below.

1. Coding of the screens

Each plane of the cube shaped screen is coded at first, where the binary code is used [9]. The coding will be done along two directions H and V which are orthogonal each other. Each direction coding will divide the plane into some slits. These slits will further divide the plane into some grids. Each grid point, regarded as a reference point, will have a special code different from other grids.

2. Coding of the specular surface

When the screen is coded, the mirror image

corresponding to each projected pattern will be observed. As a result, the specular surface is also coded. We noticed that there is a correspondence relation between a point on the specular surface and the corresponding grid point of the screen, that is, they have a same code.

3. Segmentation of the specular surface

By checking the space continuity of the observed coded image, the specular surface can be divided into several areas. In each area the space continuity of the normal will be held.

4. Creation of 3D data.

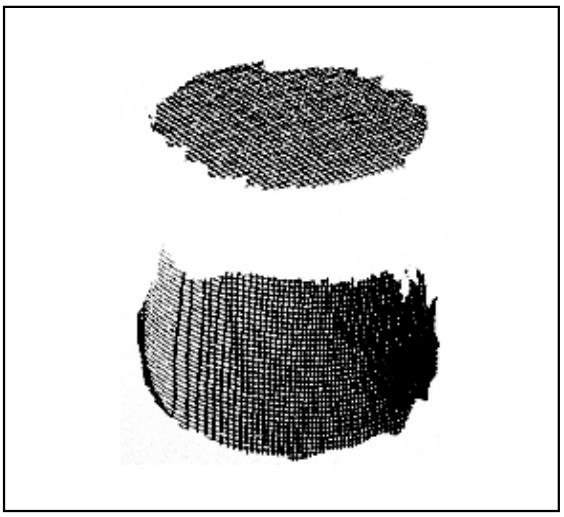

Fig.12 Wireframe

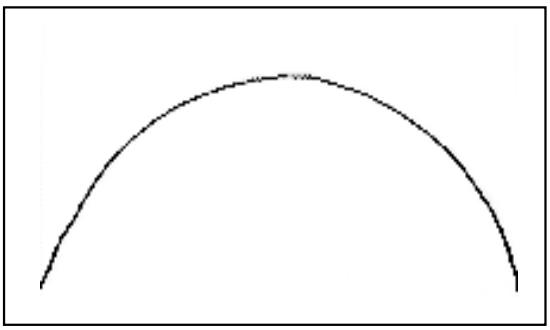

Fig.13 Cross section

To each segmented area, the above proposed methods will be used to reconstruct the specular surface.

We tested our **HU**'method on some real specular objects. Only one example is represented here. The tested specular object is an aluminum can which has a shape of cylinder. The aluminum can is 8 cm in diameter and is set in the position 100 cm away from the camera. The experimental results are shown in Fig.12 and Fig.13. Where Fig.12 gives a wireframe display of the reconstructed surface and Fig.13 gives a cross section one. The recovered cylinder has a diameter of 7 cm. The relative error is about 15%. Considering that the estimation error of seed point and the calibration error may exist, the result is acceptable.

6 Conclusion

In this paper, we presented a new method to recover specular surfaces. We show that the problem can be formulated as a constrained optimization problem. To verify the proposed methods, a prototype system has been implemented. In this system, we use an active method to simulate surrounding environment. It should be pointed out that when the position information of the surrounding environment is known, the proposed method is essentially a passive method.

7 References

[1] G. J. Klinker, et al.:"The measurement of highlightsm in color images", International Journal of Computer Vision, Vol.2, No.1, pp. 7-32 (1979).

[2] R. Bajcsy, et al.:"Color image segmentation with detection of highlights and local illumination induced by inter-reflections", Proc. 10th Int. Conf. Pattern Recognition, pp. 785-790 (1990).

[3] K. Koshikawa:"A polarimetric approach to shape understanding of glossy objects", Proc. 6th Int. Joint Conf. Artificial Intelligence, pp. 493- 495 (1979).

[4] K. Ikeuchi:" Determining surface orientations of specular surfaces by using the photometric stereo method ", IEEE Trans., Vol.PAMI-3, No.6, pp. 661-669 (1981).

[5] A. C. Sanderson, et al.:" Structured highlight inspection of specular surfaces ", IEEE Trans., Vol.PAMI - 10, No.1, pp. 44-55 (1988).

[6] S. K. Nayar, et al.:"Specular surface inspection using structured highlight and gaussian images", IEEE Trans., Vol.RA-6, No.2, pp. 208-218(1990).

[7] S. K. Nayar, et al.:"Determining shape and reflectance of hybrid surfaces by photometric sampling", IEEE Trans., Vol.RA-6, No.4, pp. 418-431 (1990).

[8] D. H. Ballard and C. M. Brown:"Computer Vision", Prentice - hall, Inc. (1982).

[9] K. Sato and S. Inokuchi:"Three-dimensional surface measurement by space encoding range imaging", Journal of Robotic System, Vol.2-1 (1985).